Journal of Crystal Growth 389 (2014) 120–133

Contents lists available at ScienceDirect

Journal of Crystal Growth

journal homepage: www.elsevier.com/locate/jcrysgro

Governing factors for the formation of 4H or 6H-SiC polytype during SiC crystal growth: An atomistic computational approach

Kyung-Han Kang [a], Taihee Eun [b], Myong-Chul Jun [b], Byeong-Joo Lee [a,*]

[a] *Department of Materials Science and Engineering, Pohang University of Science and Technology, Pohang 790-784, Republic of Korea*
[b] *SiC Material Research Team, Research Institute of Industrial Science and Technology, Pohang 790-600, Republic of Korea*

ARTICLE INFO

Article history:
Received 11 October 2013
Received in revised form
20 November 2013
Accepted 1 December 2013
Available online 14 December 2013

Keywords:
A1. Defects
A1. Atomistic simulation
A2. Crystal growth
B2. SiC
A1. Biaxial strain

ABSTRACT

The effects of various process variables on the formation of polytypes during SiC single crystal growths have been investigated using atomistic simulations based on an empirical potential (the second nearest-neighbor MEAM) and first-principles calculation. It is found out that the main role of process variables (temperature, surface type, growth rate, atmospheric condition, dopant type, etc.) is not to directly change the relative stability of SiC polytypes directly but to change the formation tendency of point defects. The biaxial local strain due to the formation of point defects is found to have an effect on the relative stability of SiC polytypes and is proposed in the present study as a governing factor that affects the selective growth of SiC polytypes. Based on the present local strain scheme, the competitive growth among SiC polytypes, especially the 4H and 6H-SiC, available in literatures can be reasonably explained by interpreting the effect of each process variable in terms of defect formation and the resultant local strain. Those results provide an insight into the selective growth of SiC polytypes and also help us obtain high quality SiC single crystals.

1. Introduction

Silicon carbide (SiC) is of fundamental and industrial interest due to its excellent electronic and mechanical properties [1–5]. With these advantages, it has been regarded as a wide-band gap semiconductor to be applicable to high-power switching, high temperature and radiation-resistant electronics [6]. SiC crystals are usually grown by chemical vapor deposition (CVD), physical vapor transport (PVT) or vapor–liquid–solid (VLS) method [7]. Generally, the SiC single crystals are grown on a {0001} seed, because Acheson crystals [8], which have a plate-like shape with a well-developed (0001) Si or $(000\bar{1})$ C face, are the only available single crystals.

More than 200 SiC polytypes are known to exist in nature [9]. They are described by different stacking of Si–C double layers along the direction perpendicular to the closed-packed plane, i.e., the cubic (111) or the hexagonal (0001) [7]. The ideal cubic (of the ZnS structure) or 3C structure follows an ABCABC… stacking sequence, whereas the stacking sequence in the [0001] direction of the hexagonal polytype 2H, for example, is ABAB.., where A, B, and C represent the three possible positions of the Si–C double layers. In order to characterize the polytypes, it is convenient to use the degree of hexagonality which is defined as the ratio of the number of hexagonal layers in the total number of layers per unit cell [7]. For example, 3C-SiC has 0% hexagonality and 2H-SiC has 100% hexagonality. Among various SiC polytypes, the practical interest is 4H and 6H-SiC structures because they can be grown as large single crystal ingot on a commercial scale [10]. 4H and 6H-SiC have hexagonal lattice in common. While 4H-SiC (50% hexagonality) has four alternating layers (ABCB) along the [0001] direction, 6H-SiC (33% hexagonality) has six alternating layers (ABCACB) along the direction.

Since SiC polytypes tend to mix with each other during crystal growth, many experiments have been performed to obtain single crystals of pure 4H [10–13] or 6H-SiC [13–16] polytype or to find the process variable that governs the growth of individual polytypes, as will be described hereafter.

The process variable first selected as the governing factor that affects the growth of individual polytypes of SiC is the temperature. The effect of temperature on the selection of SiC polytypes is rather clear and the formation efficiency of various SiC polytypes can even be presented in a functional form of temperature. The formation of 3C-SiC at low temperatures and the formation of the other polytypes at high temperatures are commonly reported [17–20]. However, among hexagonal-SiC polytypes, the 6H-SiC tends to be formed more easily than the 4H-SiC polytype at higher temperatures [17,18], which indicates that the hexagonality of the SiC crystals is not a monotonic function of temperature.

The outermost atomic layer, Si (Si-face) or C (C-face), covering the SiC (0001) surface has also been selected by several groups [21–25] as a governing factor that has an influence on the growth of polytypes. It is found that 6H-SiC grows on the Si-face, whereas

---

[*] Corresponding author. Tel.: +82 54 279 2157; fax: +82 54 279 2399.
E-mail address: calphad@postech.ac.kr (B.-J. Lee).

0022-0248/$ - see front matter © 2013 Elsevier B.V. All rights reserved.
http://dx.doi.org/10.1016/j.jcrysgro.2013.12.007

4H-SiC grows on the C-face [21–25]. The difference in the surface energy between the C-face and Si-face is thought to have influence on the selective growth of SiC polytypes [21]. In spite of the strong influence of face, it is also found that 6H-SiC tends to grow on C-face at low growth rate [25], which indicates that the crystal growth rate is also a factor that governs the growth of polytypes. However, its effect is non-decisive. Contrary to the above observation (decreasing hexagonality with decreasing growth rate [25]), a growth of 3C-SiC and hexagonal-SiC at high and low growth rates, respectively (decreasing hexagonality with increasing growth rate), has also been reported [17]. The deviation of Si:C ratio in growing atmosphere from ideal value (one) seems to have a similar non-decisive effect on the growth of polytypes. For example, in a C-rich condition, the formation of 4H [26] or 3C-SiC [27] are reported. In a sense that the 4H-SiC has a higher hexagonality than 6H-SiC while the opposite occurs for the 3C-SiC, the formation of both 4H and 3C-SiC in the same C-rich condition should be interpreted as that the effect of Si:C ratio in the growing atmosphere is non-decisive.

In addition to the above-mentioned process variables, the effect of doping elements on the growth of polytypes also needs to be examined. For example, the formation of both 4H [28–31] and 6H-SiC [32] have been reported with a doping of a common p-type dopant, Al. On the other hand, an enhanced formation of 4H [33–36] or 3C-SiC [37] has been reported with a doping of a common n-type dopant, N. In the case of 4H-SiC formation [33–36], the N-doping increased the formation tendency of 4H-SiC over 6H-SiC [33] or over 6H and 15R-SiC [34–36]. However, in case of 3C-SiC [37], the formation efficiency of 3C-SiC is reported to increase at the expense of 6H and 15R-SiC, with increasing doping level of nitrogen [37], which is opposite to the previous information [33–36] from the viewpoint of hexagonality.

Besides the above-mentioned effects of process variables, the effects of native point defects such as carbon or silicon vacancy are also reported [38,39]. In an experiment [38], a smaller number of carbon vacancies but a larger number of silicon vacancies are observed in samples with increasing hexagonality. On the other hand, a first-principles (FP) calculation [39] reports that 4H and 6H-SiC are the most stable polytype under a high concentration (10%) of carbon vacancies and silicon vacancies, respectively. It should be also mentioned here that there is an effort to interpret the selective growth of various polytypes in terms of driving force changes that originate from local strain due to differences in thermal expansion between the epilayer and substrate, injection of interstitials and stacking faults, doping-induced differences in lattice constant or electronic effects [40]. Since its influence on the growth of polytypes is not clearly known, the effects of local strain need to be systematically investigated.

It has been shown that the effects of various process variables and native defects on the growth of SiC polytypes are mostly non-decisive and more systematic investigations are required. Since the growth of polytypes is a materials phenomenon that occurs on an atomic scale, theoretical atomistic approaches would be highly required for the systematic investigation to find governing factors for the formation of SiC polytypes. Due to the large numbers of atoms involved during the crystal growth, atomistic simulations (Molecular Dynamics (MD) and Molecular Statics (MS)) based on (semi-)empirical interatomic potentials need to be considered in addition to the first-principles (FP) calculation. In this case, the quality of the interatomic potential is essential for the reliability of simulations.

Indeed, several interatomic potentials have been developed for the SiC system, including Pearson [41], Tersoff [42–45], Brenner [47–49], modified embedded-atom method (MEAM) [50], and an analytical bond-order (ABO) [51] potentials. Most of the previously developed potentials reproduce bulk properties or formation energies of various point defects in 3C-SiC fairly well. However, none of them has been applied to the crystal growth of SiC polytypes. To the best of our knowledge, only a modified Brenner potential [47] had been used to perform MD simulations for amorphous-to-crystalline transition in 4H-SiC [49]. At the beginning of the present study, an attempt was made to perform a SiC crystal growth simulation using the Tersoff, ABO and MEAM potentials. No attempt was made using the other potentials because it was not known whether those potentials could describe hexagonal SiC structures as well as the 3C structure and some materials properties (elastic properties) of 3C-SiC calculated using those potentials were not in good agreement with experiments. In the crystal growth simulation using the Tersoff and ABO potentials, no crystallization could be observed in a wide range of temperature, and partially crystallized structures with lots of defects could only be obtained in the simulation using the MEAM potential. Those preliminary studies raised a necessity of developing a new potential that can make the SiC crystal growth simulation feasible.

As a part of a long-term research to obtain high quality SiC single crystals, the purpose of the present study is to investigate the governing factors for the selective growth of 4H or 6H-SiC polytypes by using atomistic approaches such as MD, MS, and FP calculations. In order to perform MD and MS simulations for SiC crystal growth, an interatomic potential for Si-C system is newly developed based on the second nearest-neighbor modified embedded-atom method (2NN MEAM) formalism [52] which has been successful for both metallic and covalent materials. The influence of various process variables on the selective growth of polytypes is investigated using MD simulations. The effect of dopants (Al, N) and native defects is investigated using MS or FP calculations in connection to the effect of local strain on the relative stability among polytypes. Section 2 briefly covers the interatomic potential development and the quality of potential. In Section 3, the governing factor that affects the selective growth of polytypes will be investigated paying attention to the influence of process variables and local strains on growing surfaces, and Section 4 is a summary.

2. Interatomic potential

2.1. Potential parameters

The 2NN MEAM formalism for pure elements and binary systems are fully documented in the literature [52–55] and will not be repeated here. The (2NN) MEAM potential for a binary system is based on (2NN) MEAM potentials for individual constituent elements. In the present work, the potential for pure Si was taken from Lee [54] without any modification. However, the potential for pure C [55] had to be modified to better describe the Si–C binary system, in the present study. The 2NN MEAM potential parameters for pure elements, Si and C, are listed in Table 1. It should be noted here that $t^{(3)}$ and ρ_0 values of pure C are different from those in the original publication [55]. Even though general features of pure C according to the modified potential are comparable with those of original potential, the present C potential is only for Si–C system, not recommended for atomistic study of pure carbon. The values of binary potential parameters are optimized so that known physical properties of the relevant binary system are reproduced as will be described in the next section. Table 2 shows the final set of Si–C binary parameters.

2.2. Calculation of physical properties

The newly developed Si–C interatomic potential is used to compute various physical properties of SiC polytypes (3C, 6H, 4H,

Table 1
2NN MEAM potential parameter sets for Si and C.

	E_c	r_e	B	A	$\beta^{(0)}$	$\beta^{(1)}$	$\beta^{(2)}$	$\beta^{(3)}$	$t^{(1)}$	$t^{(2)}$	$t^{(3)}$	C_{min}	C_{max}	ρ_0
Si[a]	4.63	2.35	0.992	0.58	3.55	2.50	0.00	7.50	1.80	5.25	−2.61	1.41	2.80	1.88
C[b]	7.37	1.54	4.446	1.18	4.25	2.80	2.00	5.00	3.20	1.44	-0.98	1.41	2.80	5.00

The units of the cohesive energy E_c, equilibrium nearest-neighbor distance r_e and bulk modulus B are eV, Å, and 10^{12} dyne/cm^2, respectively. The reference structures of Si and C are diamond structure.

[a] Ref. [54].

[b] Ref. [55].($t^{(3)}$ and ρ_0 values are temporarily changed in the present work).

Table 2
2NN MEAM potential parameter set for the Si–C binary system.

MEAM parameter	Si–C
Reference state	ZnS_B3
E_c	$0.5E_c^{\mathrm{Si}}+0.5E_c^{\mathrm{C}}-0.3753$
r_e	1.8877
B	2.30
d	$0.5d^{\mathrm{Si}}+0.5d^{\mathrm{C}}$
$\rho_0^{\mathrm{Si}} : \rho_0^{\mathrm{C}}$	1.88: 5
C_{min} (Si–C–Si)	2.00
C_{min} (C–Si–C)	0.64
C_{min} (Si–Si–C)	1.41
C_{min} (C–C–Si)	1.41
C_{max}(Si–C–Si)	2.80
C_{max} (C–Si–C)	1.00
C_{max} (Si–Si–C)	2.80
C_{max} (C–C–Si)	2.80

The units of the cohesive energy E_c, equilibrium nearest-neighbor distance r_e and bulk modulus B are eV, Å, and 10^{12} dyne/cm^2, respectively.

and 2H-SiC) in order to evaluate its reliability. As well as the properties used for parameter optimization, temperature and pressure dependent properties of SiC polytypes are presented in this section, in comparison with experimental information or other calculations. All calculations are performed with a radial cutoff distance, 4.0 Å, which is between the second and third nearest-neighbor distances.

Tables 3, 4, 5, and 6 show calculated bulk properties of 3C, 6H, 4H, and 2H-SiC structures, respectively, in comparison with literature data (experimental information [56–69], FP calculations [70–80], and other empirical potentials [41–51]). Most properties of 3C-SiC are reproduced in a good agreement with experimental information by the present potential, except C_{44} which is lower than experimental value (Table 3). Generally, lattice parameters and elastic properties are reproduced fairly well for all the 3C and hexagonal structures. According to the present potential, 3C has the lowest energy, and then 6H, 4H and 2H in increasing order of energy. All the other empirical potentials show the same order. However, it should be mentioned that first-principles calculations report 4H as the most stable structure and then, 6H, 3C and 2H [70–82].

The temperature and pressure dependences of the volume of 3C-SiC are also available, and comparisons between the present calculation and experiments are made in Fig. 1(a) and (b). The changes of lattice parameters of 6H-SiC along temperature are experimentally reported and are compared with the present calculation in Fig. 2. It is shown that the agreement is good especially at high temperature (around 1600 K), above which crystal growth is performed.

It has been shown that the present 2NN MEAM interatomic potential can reproduce various fundamental physical properties of SiC polytypes reasonably well, except elastic constants of hexagonal-SiC. Even though many more properties would have to be further investigated using the present potential, it is hoped that the present potential would be suitable for the investigation of governing factors that affect the growth of SiC polytypes.

3. Investigation of governing factors

3.1. Influence of process variables (MD simulation)

The Si–C potential described in the previous section is used to a series of MD simulations to find the effect of various process variables (temperature, surface face, growth rate, Si:C ratio) on the growth of SiC polytypes. The MD simulation is performed in a simulation box shown in Fig. 3, with a two-dimensional periodic boundary condition along directions parallel to {0001} surface. A thin hexagonal-SiC substrate is placed on the bottom of the simulation box. The substrate is composed of three Si–C double layers of 4H-SiC (ABAC…) with lattice constants that correspond to those of bulk 4H-SiC at simulation temperatures. Since layer structure is not complete (the number of layers is not four, and bottom and top layers are C and Si single layers, respectively), the layer structure could be easily changed into other structures during crystal growth simulation. The bottom layer is fixed during the simulation to prevent the substrate from moving and to remove any bottom surface effects. The ad-atoms are randomly positioned at a distance of ten nanometers from the substrate surface along the [0001] direction, and are given an initial velocity (V_Z) as shown in Fig. 3. The initial velocity of each atom toward the substrate surface corresponds to the substrate temperature and can be calculated from the incidental (thermal) energy by the following expression:

$$V_z=\sqrt{\frac{2K_i}{M}} \tag{1}$$

where K_i represents the incidental kinetic energy which is converted into thermal energy ($1/2kT$) based on the substrate temperature and M is the atomic mass.

Experimentally, hexagonal-SiC single crystals (4H or 6H) are been grown in a temperature range of 2100–2250 °C and in an atmosphere containing Si_2C, SiC_2, C_3 and Si molecules with an overall Si:C ratio close to one [13,26,27,89]. C-face seeds are used to obtain 4H-SiC while both C and Si-face seeds can be used to obtain 6H-SiC [13]. The typical growth rate is several hundred μm/h, for example, 220 (μm/h) [90], which corresponds to about 6×10^{-11} nano-meter/pico-seconds.

In the present study, the effect of each process variable is investigated by comparing the simulated layer structure for a given reference set of process variables with the ones obtained by changing each variable one by one. Hereafter, the reference structure means what obtained under the reference condition set. In order to determine the reference condition set, the effect of some process variables

Table 3
Bulk properties of 3C-SiC structure, calculated using the present 2NN MEAM potential, in comparison with experimental data, FP calculations and other empirical potentials.

	Property	2NN MEAM	Exp.	First-principles	Empirical potentials
3C-SiC (ZnS type)	Lattice parameter (Å)	4.3595	4.3596[a]	4.344[h],4.36[i], 4.3367[j] 4.36[k],	4.19[l],4.321[m],4.280[n], 4.307[o], 4.280[p],4.349[q], 4.360[r], 4.3597[t],4.359[u]
	Heat of formation (eV $atom^{-1}$)	-0.3753	-0.34[a]–0.3753[b]		
	Bulk modulus (10^{12} dyne/cm^2)	2.30	2.25[c], 2.50[d]	2.22[h],2.16[i], 2.18[j],2.29[k]	9.9[l],2.24[m],2.31[o],2.41[p], 2.24[q],2.35[r],2.24[u]
	C_{11} (10^{12} dyne/cm^2)	3.97	3.9[c]	3.90[h],3.84[i], 3.85[i],3.72[j]	10.95[l],4.37[m],4.15[n], 4.26[o],4.47[p],2.43[q], 2.54[r],4.02[t],3.82[u]
	C_{12} (10^{12} dyne/cm^2)	1.47	1.42[c]	1.34[h],1.32[i], 1.35[j],1.57[k]	9.37[l],1.18[m],1.13[n], 1.34[o,p], 2.15[q],2.25[r], 1.16[t],1.45[u]
	C_{44} (10^{12} dyne/cm^2)	1.36	2.56[c]	2.53[h],2.41[i], 2.57[j],2.56[k]	6.06[l],3.11[m],2.11[n],2.80[o], 2.93[p],0.62[q],0.66[r], 2.15[t], 2.40[u]
	ε (10^{-6}/K) [100 – 1000 K]	4.3	2.0 ~ 4.5[e]		3[s]
	C_p (J/mol K) [500–1000 K]	49.6	40.1 ~48.1[f]		52.13[s]
	Melting point (K)	2600	2820[g]		

[a] Ref. [56].
[b] Ref. [57] (CALPHAD).
[c] Ref. [58].
[d] Ref. [59].
[e] Ref. [60].
[f] Ref. [61].
[g] Ref. [62].
[h] Ref. [70].
[i] Ref. [71].
[j] Ref. [72].
[k] Ref. [73].
[l] Ref. [41].
[m] Ref. [42].
[n] Ref. [43].
[o] Ref. [44].
[p] Ref. [45].
[q] Ref. [46].
[r] Ref. [47].
[s] Ref. [48].
[t] Ref. [50].
[u] Ref. [51].

Table 4
Bulk properties of 6H-SiC structure, calculated using the present 2NN MEAM potential, in comparison with experimental data, FP calculations and other empirical potentials.

	Property		2NN MEAM	Exp.	First-principles	Empirical potentials
6H-SiC	Lattice parameter (Å)	*a*	3.067	3.073[b]	3.074[g]	3.051[l],3.022[m], 3.078[n],3.078[o]
		c	15.246	15.118[b]	15.100[g]	15.012[l],14.868[m], 15.146[n],15.145[o]
	Energy relative to 3C (meV $atom^{-1}$)		4.3		-1.8[f],-1.6[g], -1.5[h],-1.3[i], -1.05[j]	0.2[l,m,n,o]
	Bulk modulus (10^{12} dyne/cm^2)		2.30	2.20[a]		
	C_{11} (10^{12} dyne/cm^2)		4.31	5.00[c],5.04[c], 5.02[d],5.01[e]	5.25[k]	5.20[l],4.69[m], 4.70[n],4.83[o]
	C_{12} (10^{12} dyne/cm^2)		1.73	0.92[c], 0.98[c], 0.95[d],1.11[e]	1.442[k]	0.97[l],0.99[m], 1.03[n],1.25[o]
	C_{13} (10^{12} dyne/cm^2)		0.86	0.52[e]	0.888[k]	0.5[l], 0.72[m], 0.64[n], 0.65[o]
	C_{33} (10^{12} dyne/cm^2)		5.13	5.64[c],5.66[c],5.65[d],5.53[e]	5.83[k]	5.61[l],4.93[m], 4.93[n],5.46[o]
	C_{44} (10^{12} dyne/cm^2)		1.11	1.68[c],1.70[c],1.69[d],1.63[e]	1.70[k]	1.93[l],1.72[m], 1.68[n],1.61[o]
	C_{66} (10^{12} dyne/cm^2)		1.29	2.03[d]	1.91[k]	2.12[l],1.85[m], 1.83[n],1.80[o]

[a] Ref. [61].
[b] Ref. [63].
[c] Ref. [64].
[d] Ref. [65].
[e] Ref. [66].
[f] Ref. [74].
[g] Ref. [75].
[h] Ref. [76].
[i] Ref. [77].
[j] Ref. [78].
[k] Ref. [79].
[l] Ref. [42].
[m] Ref. [43].
[n] Ref. [50].
[o] Ref. [51].

are roughly examined in preliminary MD runs. First, preliminary simulations are carried out in a wide range of temperature, seeking the temperature range that generates reasonable growth of crystals. It is found out that the crystals grown at 2300 K or below involve too many defects to analyze the crystalline structure correctly. On the other hands, it is hard to observe crystal growth at or above 2600 K, probably because the temperature, 2600 K, is close to the melting point of SiC according to the present potential (see Table 3). Between

Table 5
Bulk properties of 4H-SiC structure, calculated using the present 2NN MEAM potential, in comparison with experimental data, FP calculations and other empirical potentials.

	Property		2NN MEAM	Exp.	First-principles	Empirical potentials
4H-SiC	Lattice parameter (Å)	*a*	3.062	3.073[a]	3.067[e]	3.032[j],3.003[k], 3.06[l],3.059[m]
		c	10.20	10.053[a]	10.068[e]	10.135[j],10.038[k], 10.227[l],10.225[m]
	Energy relative to 3C (meV atom^{-1})		5.9		−2.5[d], −1.8[e], −1.9[f], −2.2[g], −1.2[h]	5.8[j],4.9[k], 5.0[l], 5.6[m]
	Bulk modulus (10^{12} dyne/cm^2)		2.30	2.20[a]		
	C_{11} (10^{12} dyne/cm^2)		4.49	5.07[b]	5.372[i]	5.04[j],4.60[k], 4.73[l],4.86[m]
	C_{12} (10^{12} dyne/cm^2)		1.93	1.08[b]	1.560[i]	0.94[j],1.00[k], 1.09[l],1.27[m]
	C_{13} (10^{12} dyne/cm^2)		0.51		1.085[i]	0.4[j], 0.64[k], 0.61[l],0.62[m]
	C_{33} (10^{12} dyne/cm^2)		5.76	5.47[b], 5.649[c]	6.050[i]	5.33[j],4.72[k], 4.89[l],5.38[m]
	C_{44} (10^{12} dyne/cm^2)		1.07	1.59[b]	1.701[i]	1.95[j],1.73[k], 1.70[l],1.62[m]
	C_{66} (10^{12} dyne/cm^2)		1.28		1.907[i]	2.05[j],1.81[k], 1.83[l],1.79[m]

[a] Ref. [61].
[b] Ref. [66].
[c] Ref. [67].
[d] Ref. [74].
[e] Ref. [75].
[f] Ref. [76].
[g] Ref. [77].
[h] Ref. [78].
[i] Ref. [79].
[j] Ref. [42].
[k] Ref. [43].
[l] Ref. [50].
[m] Ref. [51].

Table 6
Bulk properties of 2H-SiC structure, calculated using the present 2NN MEAM potential, in comparison with experimental data, FP calculations and other empirical potentials.

	Property		2NN MEAM	Exp.	First-principles	Empirical potentials
2H-SiC	Lattice parameter (Å)	*a*	3.055	3.08[a],3.079[b]	3.044[g],3.077[g]	
		c	5.122	5.04[a],5.052[b]	4.995[g],5.053[g]	
	Energy relative to 3C (meV atom^{-1})		8.5		1.1[c],2.6[d],2.7[e]	7.0[h],5.9[i], 6.1[j],6.7[k]
	Bulk modulus (10^{12} dyne/cm^2)		2.30			
	C_{11} (10^{12} dyne/cm^2)		4.72		5.200[f]	5.07[h],4.65[i], 4.76[j],4.83[k]
	C_{12} (10^{12} dyne/cm^2)		2.20		1.452[f]	0.97[h],1.03[i], 1.12[j],1.24[k]
	C_{13} (10^{12} dyne/cm^2)		0.02		0.89[f]	0.42[h],0.65[i], 0.60[j],0.67[k]
	C_{33} (10^{12} dyne/cm^2)		6.74		5.852[f]	5.32[h],4.75[i], 4.86[j],5.40[k]
	C_{44} (10^{12} dyne/cm^2)		1.04		1.70[f]	1.96[h],1.74[i], 1.70[j],1.64[k]
	C_{66} (10^{12} dyne/cm^2)		1.26		1.837[f]	2.05[h],1.81[i], 1.83[j],1.80[k]

[a] Ref. [68].
[b] Ref. [69].
[c] Ref. [76].
[d] Ref. [77].
[e] Ref. [78].
[f] Ref. [79].
[g] Ref. [80].
[h] Ref. [42].
[i] Ref. [43].
[j] Ref. [50].
[k] Ref. [51].

2400 K and 2500 K, reasonable crystal growth can be observed and these two temperatures which are close to experimental temperature range are chosen as the reference temperature. Concerning the surface component, it is decided to choose the Si-face for the substrate. This is because Si-face seeds generate fewer defects than C-face seeds during preliminary growth simulations. The overall ratio between Si and C in the atmosphere is maintained to be one for the reference condition. As mentioned above, the growth of crystals is simulated by sending individual ad-atoms from the top of the simulation box toward the surface at a given velocity determined by the temperature. The number of ad-atoms sent to the surface per time yields the growth rate. In the present simulation, one ad-atom per pico-second is chosen as the reference condition. This corresponds to a growth rate of about 10^{-4} nano-meter/pico-seconds, which is larger than the typical experimental growth rate by about six orders. Even though the simulated growth rate is too large compared to experiments, it is almost the minimum growth rate that can be achieved using a reasonable simulation time. This big difference in the growth rate should be kept in mind when interpreting the simulation results, and relative changes between the reference structure and structures with varied conditions need to be paid more attention rather than the absolute results under individual conditions.

As a reference to examine the effect of process variables, the crystal growth is simulated over a Si-face substrate by sending each of Si and C ad-atom toward the substrate per 2 pico-seconds, at 2400 K and at 2500 K. The resultant structures are presented in Fig. 4(a). It should be noted here that even though 4H and 6H-SiC are interesting polytypes among the four polytypes considered, only 3C and 2H structures are obtained during the simulation. A great amount of efforts are made to obtain 4H or 6H structures, but without success. Before continuing simulations by changing each process variable, one more needs to be confirmed. In experiments, as mentioned already, the constituents of

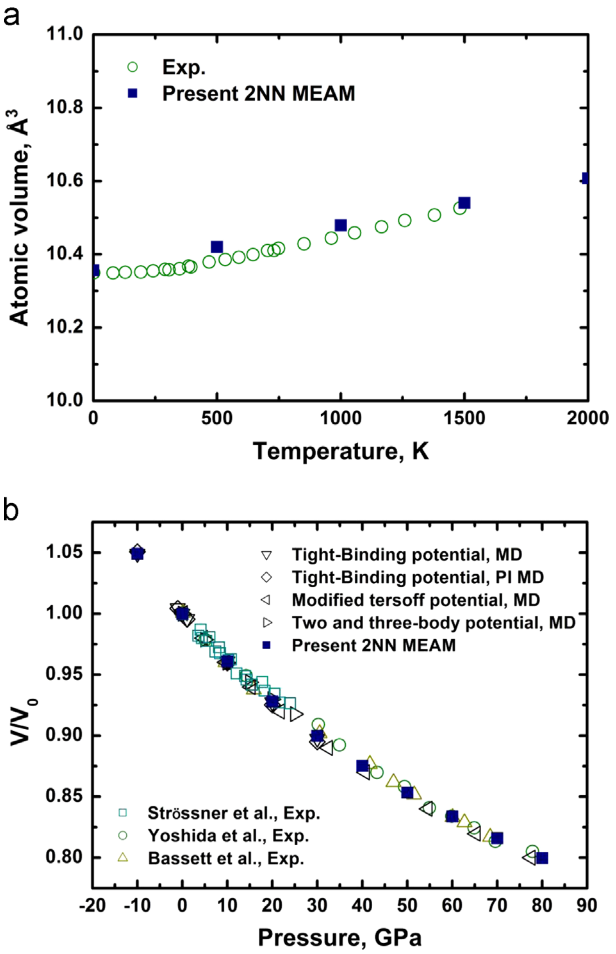

Fig. 1. Calculated (a) atomic volume vs. temperature and (b) pressure–volume relation of 3C-SiC in comparison with experimental data [63,83–85] and other calculations [86–88].

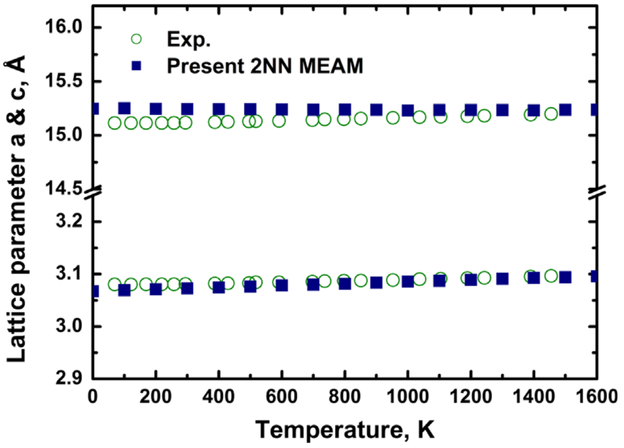

Fig. 2. Calculated lattice parameters *a* and *c* of 6H-SiC vs. temperature, in comparison with experimental data [63].

the growth atmosphere are molecules, while those in simulations are pure atoms. The selection of ad-atoms as the growing unit is only for the convenience of simulation. It is necessary to confirm that the simulations using ad-atoms yield the same results as those using ad-molecules. In order to perform simulations using ad-molecules, information for the ratio among constituent molecules is needed. To obtain such information, a CALPHAD [91,92] type thermodynamic calculation is performed for the overall composition of Si:C = 1:1 in a temperature range including 2400 and 2500 K using ThermoCalc [93] and SUB97 [94] database. The result is shown in Fig. 5. This result is used to perform another set of growth simulations using ad-molecules, as shown in Fig. 4(b). It can be confirmed that the same polytypes (mostly 3C at 2400 K and 2H at 2500 K) as those grown using ad-atoms are obtained when using ad-molecules.

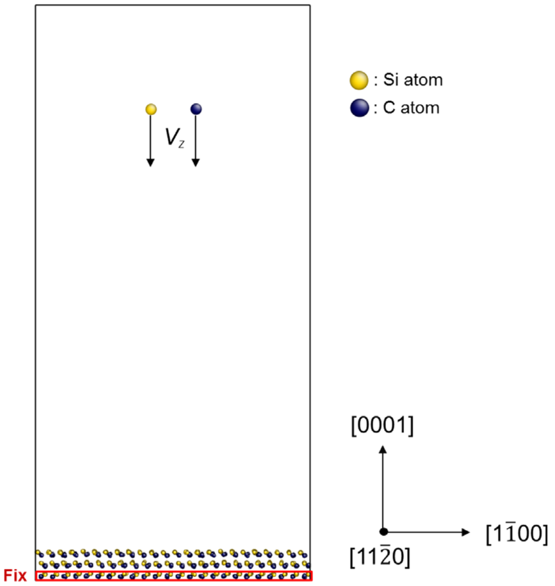

Fig. 3. Side view of simulation box for the crystal growth. One bottom layer (inside the red box) is fixed. Yellow (light gray) and navy (dark gray) spheres represent Si and C atoms, respectively. (For interpretation of the references to color in this figure legend, the reader is referred to the web version of this article.)

Based on the results presented in Fig. 4, further simulations are continued using ad-atoms by changing each process variable one by one. All the results are presented in Fig. 6. When C-face is used instead of Si-face, no change is observed compared to the reference structures, that is, mostly 3C is obtained at 2400 K and 2H is obtained at 2500 K (Fig. 6(a)). On the other hands, when the growth rate is reduced to a half level, the 2400 K sample initially grows into 2H structure even though it eventually grows into 3C structure, as shown in Fig. 6(b). Fig. 6(c) shows that as in the case when the surface is changed from Si-face to C-face (Fig. 6(a)), no relative change from the reference structures is observed when the growth atmosphere is changed to a Si-rich condition (Si:C = 1.1:1). In the case of C-rich atmosphere (Si:C = 1:1.1), however, 3C growth is observed even at 2500 K as well as at 2400 K as shown in Fig. 6(d).

In summary, in all cases considered, 2H is grown at higher temperature, 2500 K, with an exception for the C-rich atmosphere where 3C is grown, and 3C is eventually grown at the relatively lower temperature, 2400 K. It has been mentioned that 2H structure is initially grown even at the lower temperature, 2400 K, if the growth rate is reduced to a half level (Fig. 6(b)). It should be emphasized here that in the initial seed (Fig. 3), only the bottom two layers form the 2H structure and the third layer from the bottom (the top layer) could initiate a growth into other structures. However, a closer look at the 2400 K samples shows that the seeds start growing into 2H structure in all samples and transform to 3C structure during the growth. The case of reduced growth rate, Fig. 6(b), is simply a case where 2H is grown to the largest amount and the transition into 3C structure occurs latest among all the cases considered. It is also shown that the grown 3C structures always involve a group of defects while the 2H structures do not, which implies that the formation of 3C and defects are closely related to each other. To understand the transition into

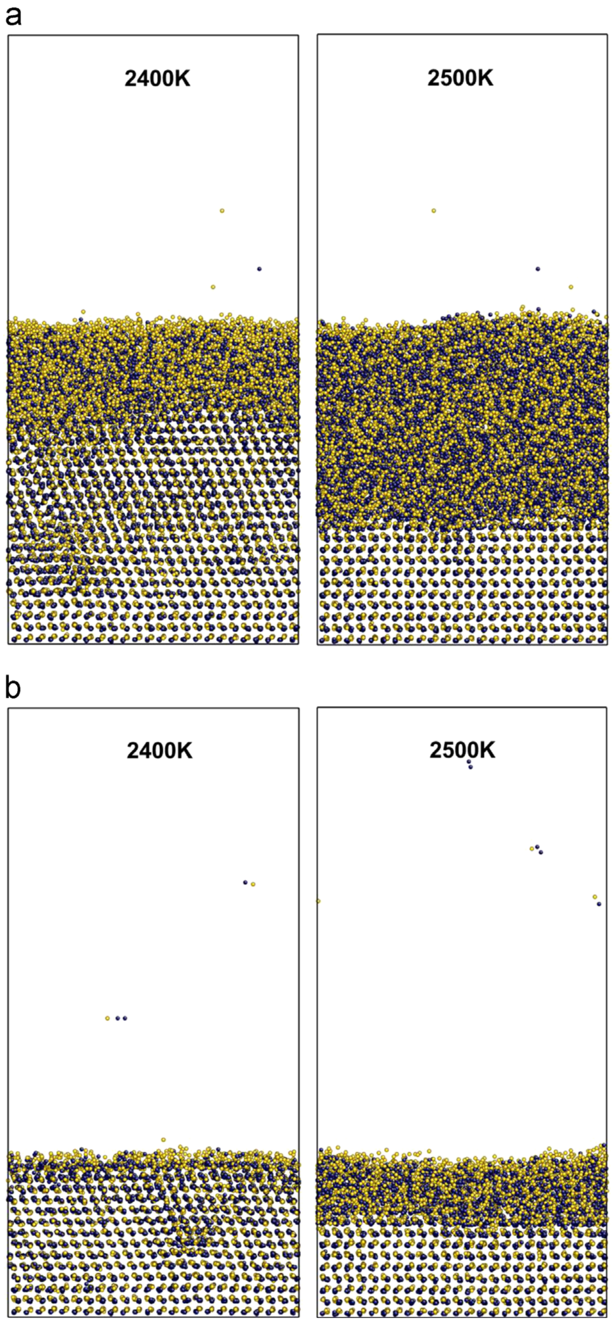

Fig. 4. Side view of grown structures under the (a) reference condition and (b) the same condition but using ad-molecules instead of ad-atoms.

3C structure, it is necessary to clarify its probable relation with defects. First, it is necessary to identify the character of the defects. The number of vertical layers along the direction parallel to the seed surface (from left end to right end of the sample) in initial seed and in the grown 2H structure is twenty-four. However, after the formation of the defects, it increases to twenty-five, which means an insertion of an extra atomic layer and implies that the group of defects shown in 3C region is an edge dislocation. Since it can be thought that a large amount of point defects may enhance the formation of dislocations, the type and number of point defects in individual layers are analyzed along the growth direction, as shown in Fig. 7.

It should be reminded that the types of probable point defects are six: two vacancies (V_{Si}, V_C), two antisite defects (Si_C, C_{Si}, where C_{Si} represents a carbon atom on a silicon site) and two interstitials (I_{Si}, I_C). It should be also mentioned that the simulated point defect densities must be much higher than experimentally measured ones because the simulated growth rate is much higher than experimental ones. Fig. 7 shows that the point defects formed during the SiC crystal growth are the two antisite defects and carbon vacancy. The number of those point defects is not changed during the growth of 2H structure at 2500 K, while it increases as the growth proceeds in the same 2H structure at 2400 K. The trend is all the same in all conditions considered. For example, the changes of point defects along the growth direction in the “2400 K low growth rate” sample where 2H portion is largest, in the “2400 K Si-rich” sample where the initial 3C region does not involve dislocation, in the “2500 K C-rich” sample where the 3C transition occurs even at 2500 K and in the “2500 K Si-rich” sample where the 3C transition does not occur are presented in Fig. 8(a), (b), (c) and (d), respectively. In all cases that show the 3C transition (Fig. 8(a)–(c)), the number of point defects increases as the growth proceeds while it remains at a constant level in the case that shows no 3C transition (Fig. 8(d)). It can be presumed that the increase of those point defects cause the transition into 3C structures and eventually the formation of dislocations.

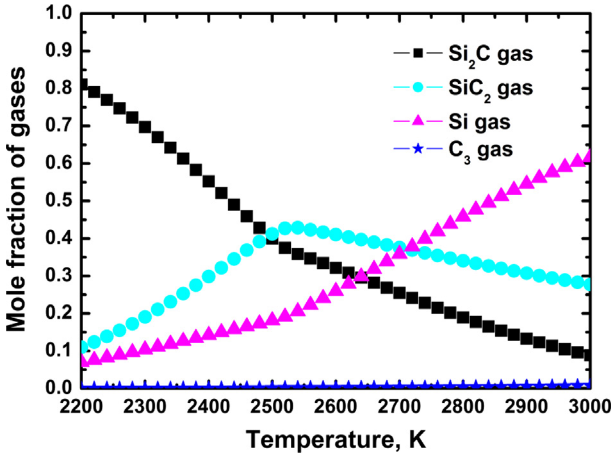

Fig. 5. The distribution of various Si–C molecules (Si_2C, SiC_2, Si, C_3) as a function of temperature, calculated using ThermoCalc [93] and SUB97 [94] database.

Based on the correlation between the increase of point defects and the occurrence of the 3C transition, the present authors conclude that the reference condition of the present study is essentially the one that prefers the growth of hexagonal SiC if defects are not included during the growth. Further, the principal factor that has a direct effect on the growth of SiC polytypes is the formation of defects. It is believed that, within the temperature of 2400–2500 K, the main role of temperature is not to change the relative stability among growing polytypes but to change the possibility of the formation of defects. That is, defects can occur relatively easily at the lower temperature where atomic diffusion may not be sufficient. At reduced growth rates, the formation of defects can be retarded because relatively sufficient time can be given for atomic diffusion which would reduce the defect formation tendency. This is believed to be the reason why 2H structure is grown larger amount under the reduced growth rate condition (Fig. 6(b)) than other cases at 2400 K. It can be also thought that the C-rich atmospheric condition increases the defect formation tendency and causes the 3C transition even at 2500 K (Fig. 6(d)).

It should be emphasized here that the above-mentioned conclusions from the present simulation (the increasing tendency of defect formation with decreasing temperature, increasing growth rate and increasing C-rich condition) are in line with experimentally observed process conditions that increase the dislocation density [90,95,96].

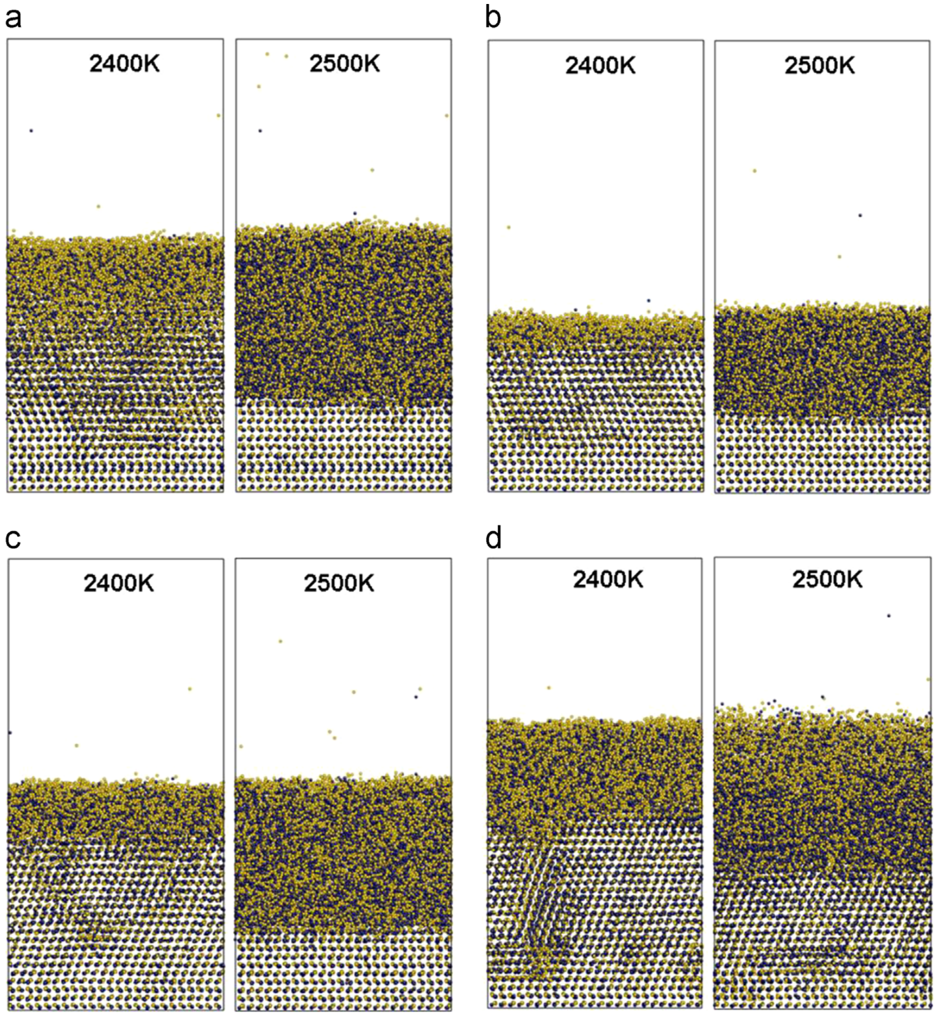

Fig. 6. Side view of grown structures under the (a) C-face, (b) low growth rate, (c) Si-rich and (d) C-rich condition.

3.2. *Influence of local strain (MS and FP calculations)*

Through the molecular dynamics simulations analyzed in the previous section, it has been concluded that the process variables may not directly change the relative stability of individual SiC polytypes. Instead, the easiness of the formation of point defects is chosen as the governing factor that determines the polytype growth, and the process variables are thought to have effects only on the easiness of the formation of point defects. The effect of temperature and the effect of growth rate on the easiness of the formation of defects could be reasonably rationalized. However, there still exist remaining questions. The first is why 3C transition is enhanced when large amount of point defects are formed, and the second is why large amount of point defects are formed under the C-rich atmospheric condition even at the higher temperature, 2500 K.

The present authors think that the presence of point defects would cause a local strain at surrounding lattices. For example, the presence of vacancies would cause a locally tensile strain, while the presence of interstitials would cause a locally compressive strain. The antisite defects Si_C and C_{Si}, are expected to cause a local compressive and tensile strain, respectively, due to the size difference between two atoms. If the local strain has an effect on the relative stability among individual SiC polytypes, the changed relative stability would be detected by the ad-atoms or molecules arriving at the growing surface, and would eventually determine the polytype growth. In order to prove the validity of the present supposition, the effect of biaxial strain parallel to {0001} faces on the relative stability of 3C and 2H is calculated, both using the present interatomic potential (that was used for the molecular dynamics simulations) and a first-principles calculation. Fig. 9(a) shows the change of potential energy of 3C and 2H films as a function of biaxial strain. Here, a zero strain means that the lattice constant is that of bulk for each structure, and the positive (negative) sign of strain means that it is tensile (compressive). It is shown that the 3C structure becomes relatively more stable than the 2H structure under any types of strain between ±5%. The abrupt decrease of the energy for 2H structure above 5% tensile stress is due to a partial reconstruction of the 2H structure and is thought to be an artifact that comes from the incompleteness of the interatomic potential. Fig. 9(a) indicates that the occurrence of any local strain due to the formation of point defects stabilizes the 3C structure over the 2H structure, causing the transition into the 3C structure as has been observed in the present molecular dynamics simulations. The first-principles calculation shows a similar trend as shown in Fig. 9(b), even though the size of the effect of strain is small compared to the empirical potential calculation. A 24-atom supercell $(1\times1\times12)$ is used in the first-principles calculation based on the projector-augmented wave (PAW) potential [97] within the density functional theory (DFT) framework [98] under the Perdew–Burke–Ernzerhof (PBE) exchange-correlation functional [99].

It can be thought that the same explanation may be applied to the relative stability between 4H and 6H structures, which could

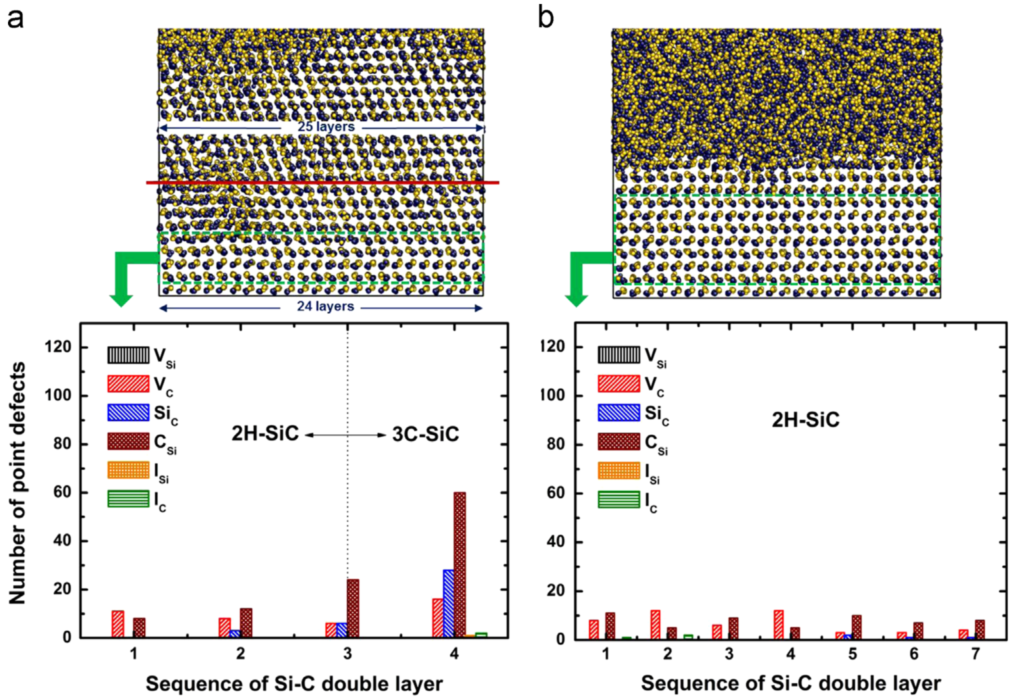

Fig. 7. Simulated distribution of point defects along each adjacent Si–C double layer toward growing direction from the seed (the part inside green box of side view) under 2400 K (left) and 2500 K (right) reference conditions. The red line in the left sample is the boundary above which the number of vertical layers changes from 24 to 25. (For interpretation of the references to color in this figure legend, the reader is referred to the web version of this article.)

not be investigated using the present molecular dynamics simulation. The calculated effect of biaxial strain on the relative stability between 4H and 6H according to the present potential and first-principles is presented in Fig. 10(a) and (b), respectively. Both calculations indicate that local tensile strain stabilizes 4H over 6H, while local compressive strain does the opposite. This means that the results of competition between 4H and 6H growth under changing process variables may be predictable if the effects of individual variables on the formation of point defects and the sign of local strain due to the formation of defects are known. Therefore, the remaining part of the present study is focused to prove the validity of the present scheme to explain and predict the competitive growth between 4H and 6H SiC polytypes under various process conditions, by interpreting the effect of available experimental process conditions in terms of defect formation and the resultant occurrence of local strains.

In order to investigate the effect of individual process variables in terms of the defect formation, one needs to know the formation tendency of all probable point defects. The formation energy of various point defects probable in the 3C-SiC structure, calculated using the present 2NN MEAM potential, first-principles and other empirical potentials, are listed in Table 7. In the present calculation, it is assumed that the chemical potential difference between Si and C ($\mu_{Si}-\mu_C$) in the SiC structure are maintained the same as that for pure elements (diamond Si and C). The calculation results from each method show some mutual discrepancies, but in overall, one may say that carbon vacancy (V_C), carbon antisite (C_{Si}) and silicon antisite (Si_C) are the main point defects that can be observed rather easily in 3C-SiC and also probably in other hexagonal structures. Such calculations of formation energy of point defects enable explanations on the results of defect analyses shown in Figs. 7 and 8, for example, why C_{Si} is dominant in the C-rich condition while V_C instead of Si_C is dominant in the Si-rich condition (see Fig. 8(c) and (d)).

Experimental information reported for the effect of temperature on the competitive growth between 4H and 6H-SiC is that the 4H structure is preferentially grown at lower temperature around 2400–2500 K [17,18]. Out of the three most probable point defects (V_C, C_{Si} and Si_C), two (V_C, and C_{Si}) are those induce locally tensile strains, and the relative stability of 4H increases with increasing amount of tensile strain as shown in Fig. 10. From those, it can be expected that the stability of 4H would increase at relatively lower temperature where the defect formation tendency during crystal growth is thought to increase. It should be mentioned here that the growth of 3C structure at lower temperature has been reported experimentally [27] and also from the present molecular dynamics simulation. However, the temperature range where the growth of 3C structure is experimentally reported (~2073 K) is much lower than 2400–2500 K. Since the present scheme for the effect of local strain on the relative stability among SiC polytypes is based on 0 K energy calculations (Figs. 9 and 10), any attempt to explain the competitive growth between 3C structure and 4H or 6H structure at finite temperatures around 2000 K would not be suitable. Only the interpretation for the competitive growth between the 3C and the 2H which is known to be formed also at low temperatures (~1973 K [17]), and between 4H and 6H that appear competitively in the same temperature range would be of physical significance.

Concerning the effect of the type of surface, that is, the preferential growth of 6H on Si-face and 4H on C-face [21–25], the present authors believe that the C-face generates more defects (a defect analysis as in Figs. 7 and 8 also shows the same tendency) inducing mostly tensile strains and stabilizes 4H structure over 6H. The growth of 6H even on the C-face at low growth rate [25] can be interpreted to be due to the slow growth that allows time for annihilation of point defects and resultant stabilization of 6H over 4H. Concerning the formation of 4H [26] or 3C [27] in a C-rich atmospheric condition, as already mentioned, it should be emphasized that the growth temperature of 3C is well below the temperature range for the growth of 4H or 6H. The point defect that can be formed under C-rich atmospheric condition is C_{Si} (see Table 7) which contributes to generate local tensile strains and eventually stabilizes 4H over 6H.

In addition to the above-mentioned process variables, the effect of doping elements, Al and N, are well reported. As already

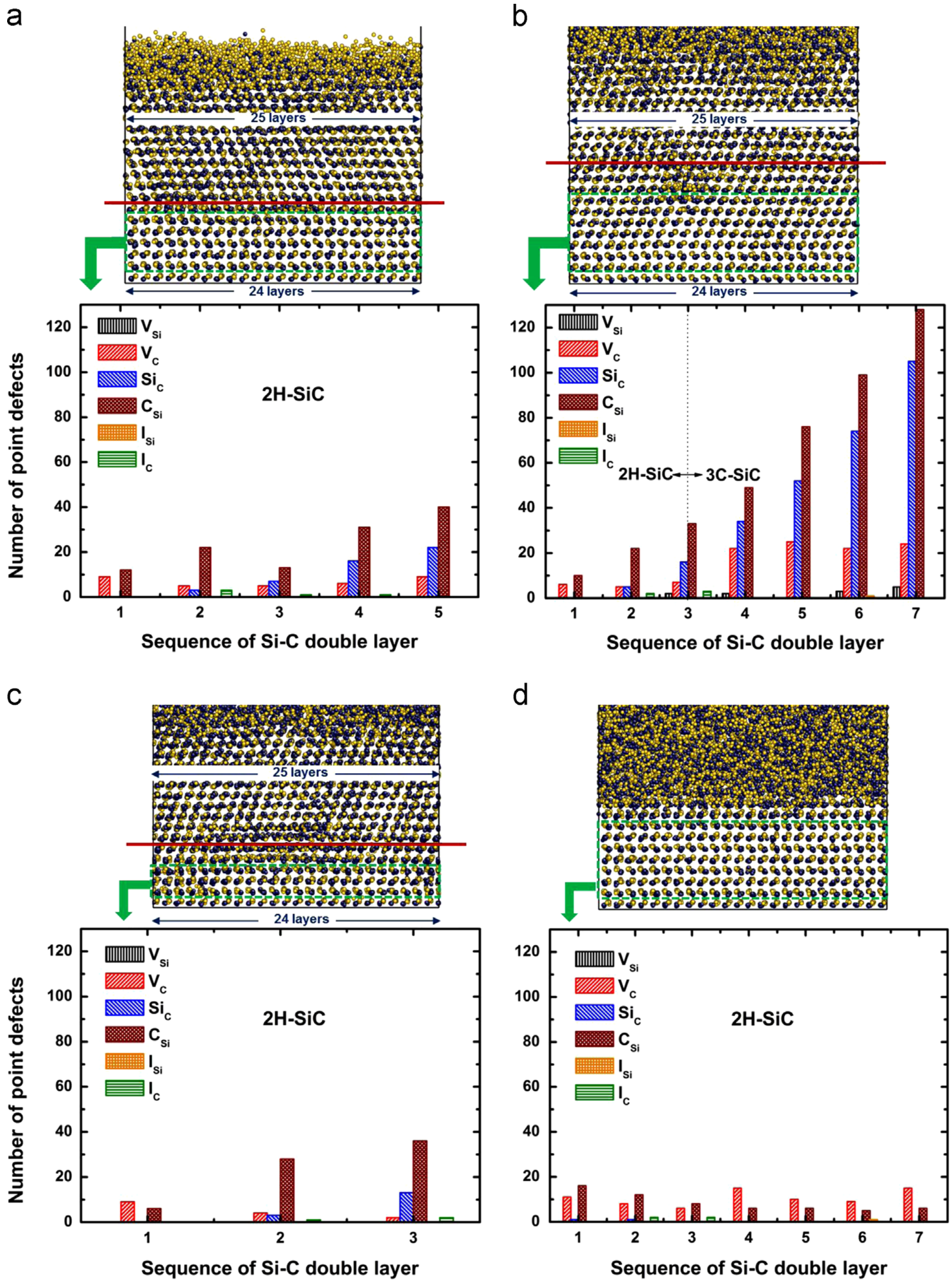

Fig. 8. Simulated distribution of point defects along each adjacent Si–C double layer toward growing direction from the seed (the part inside green box of side view) under (a) 2400 K low growth rate, (b) 2400 K Si-rich, (c) 2500 K C-rich and (d) 2500 K Si-rich conditions. Red line is the boundary between 24 and 25 vertical layer structures. (For interpretation of the references to color in this figure legend, the reader is referred to the web version of this article.)

mentioned in the introduction of the present manuscript, the effect of Al doping is non-decisive, generating both 4H [28–31] or 6H [32] depending on the process condition. Similarly, the effect of N looks non-decisive, with the preferential formation of 4H over 6H [33–36], or the preferential formation of 3C over 6H [37], also depending on the process condition. To rationalize all the above experimental information, one needs to know the effect of doping elements on the generation of local strains or the formation of other defects. For this, it is necessary to know which sites (Si or C site) will the dopant atoms (Al or N) be positioned in the SiC structure first. Since Si–C–Al or N ternary potential is not available, a first-principles calculation is used to calculate the heat of substitution for Al or N in the 3C-SiC structure. The result obtained using a 64-atom supercell (4 × 4 × 4) is presented in Table 8. It is shown that Si site is the energetically favorable site for Al atoms and C site is the one for N atoms, in agreements with another first-principles calculation [103]. It is also found that the Al substitution for Si site generates a compressive strain while the N substitution for C site generates a tensile strain.

The local strains generated by the substitution of doping elements can have effects on the relative stability between 4H and 6H-SiC. However, there is an indirect evidence for the formation of other defects such as vacancy and interstitial induced by the Al-doping [30]. It should be reminded here that another probable point defect that can be associated with the Al doping is the carbon vacancy, V_C. Therefore, the change in the formation energy of V_C, when it is

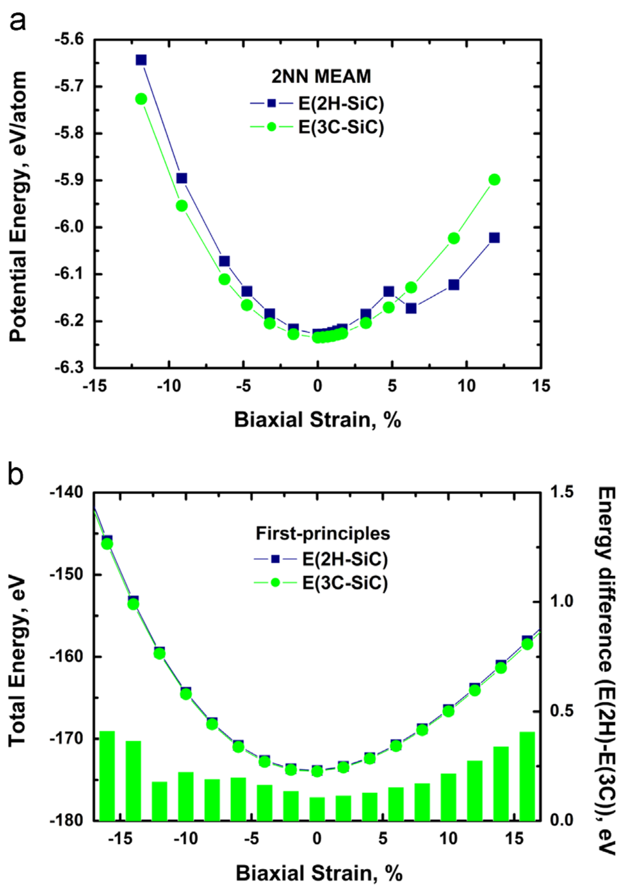

Fig. 9. Effects of (0001) biaxial strain on the relative stability of 2H and 3C-SiC structures at 0 K, according to the (a) 2NN MEAM and (b) first-principles calculations. The histogram in (b) represents the energy difference between the two structures.

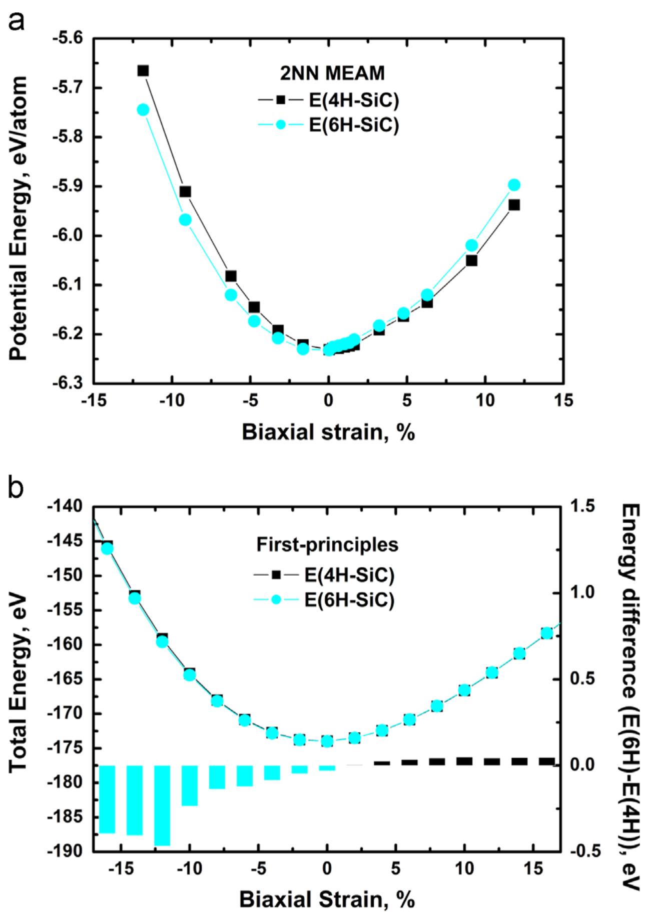

Fig. 10. Effects of (0001) biaxial strain on the relative stability of 4H and 6H-SiC structures at 0 K, according to the (a) 2NN MEAM and (b) first-principles calculations. The histogram in (b) represents the energy difference between the two structures.

Table 7
Formation energy of various point defects probable in the 3C-SiC structure, calculated using the present 2NN MEAM, first-principles and other empirical potentials.

Property	Defect type	2NN MEAM	First-principles	Empirical potential
Vacancy formation energy (eV)	V_{Si}	4.52	8.01[a],8.2[b],8.1[c]	4.67[d],4.55[e]
	V_C	1.44	5.11[a],4.5[b], 4.2[c]	1.39[d],1.90[e]
Antisite formation energy (eV)	C_{Si}	2.02	4.06[a],3.8[b], 3.4[c]	4.43[d],2.42[e]
	Si_C	4.63	4.46[a],4.6[b]	5.05[d],2.48[e]
Interstitial formation energy (eV)	C_{TC}	2.67	7.78[a],12.4[b]	6.02[d],12.63[e]
	C_{TSi}	8.74	7.2 [a],10.0[b]	5.69[d],9.38[e]
	Si_{TC}	3.61	4.8[a],13.3[b]	2.60[d],17.55[e]
	Si_{TSi}	4.38	7.34[a],13.6[b]	5.40[d],17.30[e]

C_{TC} denotes tetrahedrally coordinated carbon interstitial surrounded by four carbon atoms.

[a] Ref. [100].
[b] Ref. [101].
[c] Ref. [102].
[d] Ref. [47].
[e] Ref. [51].

formed on a neighboring site of a dopant Al atom instead of in pure SiC is estimated using a first-principles calculation. The result is presented also in Table 8. It is shown that the formation energy of V_C is reduced from 4.45 to 1.93 eV if it is formed on a neighboring site of Al. Similar tendency is expected from N doping for the formation energy of V_{Si} (a reduction from 7.47 to 5.21 eV), but the degree of reduction is less significant compared to that for V_C. The present authors believe that the Al doping induces a tensile strain due to the enhanced formation of neighboring carbon vacancies rather than a compressive strain due to the Al size effect, and eventually stabilizes and promotes the formation of 4H rather than 6H. The case where 6H is reported to form [32] is much different from the cases for the 4H [28–31], in processing method, temperature and growth rate. A chemical vapor deposition method (one with the highest purity) is used instead of solid state reaction, and the temperature and growth rate is lower by about 1000 K and two orders of magnitude, respectively. It is further reported that almost no defect is observed in the grown film of this case, probably because of the high purity and the low growth rate. The present authors think that the defect-free growth condition with the compressive strain due to the Al substitution could stabilize the 6H structure more than the 4H structure.

N doping is believed to induce local tensile strains due to the size effect and to promote the growth of 4H rather than 6H, as experimentally reported [33–36]. However, the report on the formation of 3C instead of 6H [37] at an equally high temperature (2473 K) needs to be clarified. A close look at the process condition for the formation of 3C indicates that the nitrogen partial pressure in this process is larger than the other cases by around two orders of magnitude. It has been experimentally reported that a large amount of N doping increases the formation tendency of defects and dislocations [37,90]. The present authors believe that the large amount of N atoms and thus created defects and dislocations made the growing surface condition to be similar to that obtained at high growth rate with large amount of defects, where 3C is usually formed [17].

Table 8

Formation energy of substitutional defects (Al or N), vacancies near the substitutional defects and vacancies in pure 3C-SiC by a first-principles calculation.

Property	Defect type	Al atom	N atom
Formation energy (eV)	Substitution for Si	1.67	6.23
	Substitution for C	7.37	-0.61
	Vacancy near substitutional defect	1.93 (V_C)	5.21 (V_{Si})
	Vacancy in pure SiC	4.45 (V_C)	7.47 (V_{Si})

Table 9

A summary and the present interpretation for the effects of process variables on 4H or 6H-SiC polytype growth.

Condition	Polytype	Temperature (K)	Growth rate (μm/h)		Interpretation
Si-face	6H[a]	2453–2653[a]			Formation of more defects and tensile strain on C-face (4H).
C-face	4H[a,b]	2453–2723[a] 2534–2564[b]	>1455[b]		Reduced formation of defects due to slow growth.(6H).
	6H[b]	2534–2564[b]	<1455[b]		
C-rich	4H[c]	2273[c]	100–1000[c]		Formation of more defects and tensile strain at low temperature (4H).
	3C[d]	1573, 1673, 2073[d]			Formation of much more defects at even lower temperatures (3C).
Al-doping	4H[e,f,g]	2173[e] 2473[f,g]		Doping level (at%) 1.67[e] 0.75[f,g]	Formation of more carbon vacancies and tensile strain (4H).
	6H[h]	1423[h]	0.25–8[h]	0.01–0.1[l]	Reduced formation of defects due to slow growth and high purity (6H).
N-doping	4H[i,j]	2398[i] 2403–2473[j]	1000[i]	N partial pressure (Torr) 2.5–4.1 (Total: 10)[i]	Tensile strain due to size effect of N (4H).
	3C [k]	2473[k]		400–760 (Total:760)[k]	Formation of more defects due to a large doping level (3C).

[a] Ref. [21].
[b] Ref. [25].
[c] Ref. [26].
[d] Ref. [27].
[e] Ref. [29].
[f] Ref. [30].
[g] Ref. [31].
[h] Ref. [32].
[i] Ref. [34].
[j] Ref. [36].
[k] Ref. [37].
[l] Estimated from experiment (Ref. [104]).

It has been shown that the local strains on the growing surface due to the formation of various defects can be the governing factor that affects the selective growth of SiC polytypes, and that the effects of various process variables can be interpreted in term of easiness of the defects as summarized in Table 9. Most of the experimental observations for the formation of SiC polytypes, especially the competitive growth of 4H and 6H-SiC, can be rationalized on the basis of the present scheme which can provide guidance for further experimental study to grow high quality SiC single crystals.

4. Conclusion

Local biaxial strains on the growing surface are found out to have an effect on the relative stability of individual polytypes of SiC crystal. It is also found out that various point defects formed during the crystal growth can be the origin of the local strains. Therefore, the role of various process variables (temperature, surface type, growth rate, atmospheric condition, dopant type, etc.) needs to be interpreted in terms of their effects on the easiness of the formation of defects and the type (tensile vs. compressive) of resultant local strain. An attempt made to explain literature information for the competitive growth between 4H and 6H-SiC confirms that the present scheme based on the defect formation and local strain can be a useful guidance in further experimental studies for selective growth of high quality SiC single crystals.

Acknowledgments

This work has been financially supported by the Pohang Steel Company (POSCO) and by the National Research Foundation (Grant no. 2011-0010033) of Korea.

References

[1] M. Bhatnagar, B.J. Baliga, Comparison of 6H-SiC, 3C-SiC, and Si for power devices, IEEE Trans. Electron Devices ED 40 (1993) 645–655.
[2] T.P. Chow, M. Ghezzo, SiC power devices, Mater. Res. Soc. Symp. Proc. 423 (1996) 9.
[3] C.E. Weitzel, K.E. Moore, Silicon carbide and gallium nitride Rf power devices, Mater. Res. Soc. Symp. Proc. 483 (1998) 111.
[4] B.J. Baliga, High voltage silicon carbide devices, Mater. Res. Soc. Symp. Proc. 512 (1998) 77.
[5] C.E. Weitzel, Silicon carbide high frequency devices, Mater. Sci. Forum 264–268 (1998) 907.
[6] Y.T. Yang, K.L. Ekinci, X.M.H. Huang, L.M. Schiavone, M.L. Roukes, C.A. Zorman, M. Mehregany, Monocrystalline silicon carbide nanoelectromechanical systems, Appl. Phys. Lett. 78 (2001) 162–164.
[7] A. Fissel, Artificially layered heteropolytypic structures based on SiC polytypes: molecular beam epitaxy, characterization and properties, Phys. Rep. 379 (2003) 149–255.
[8] A.G. Acheson, English Patent no. 17911, 1892.
[9] N.W. Jepps, T. Page, in: P. Krishna (Ed.), Progress in Crystal Growth and Characterization, 7, Pergamon, Oxford, 1983, p. 259.
[10] R. Yakimova., E. Janzén, Current status and advances in the growth of SiC, Diamond Relat. Mater. 9 (2000) 432–438.
[11] R. Yakimova, M. Syväjärvi, T. Iakimov, H. Jacobsson, R. Råback, A. Vehanen, E. Janzén, Polytype stability in seeded sublimation growth of 4H-SiC boules, J. Cryst. Growth 217 (2000) 255–262.

[12] E.Y. Tupitsyn, A. Arulchakkararvarthi, R.V. Drachev, T.S. Sudarshan, Controllable 6H-SiC to 4H-SiC polytype transformation during PVT growth, J. Cryst. Growth 299 (2007) 70–76.

[13] K. Semmelroth, N. Schulze, G. Pensl, Growth of SiC polytypes by the physical vapour transport technique, J. Phys.: Condens. Matter 16 (2004) S1597–S1610.

[14] H.J. Rost, D. Siche, J. Dolle, W. Eiserbeck, T. Müller, D. Schulz, G. Wagner, J. Wollweber, Influence of different growth parameters and related conditions on 6H-SiC crystals grown by the modified Lely method, Mater. Sci. Eng. B 61–62 (1999) 68–72.

[15] W.S. Yoo, S. Nishino, H. Matsunami, Single crystal growth of hexagonal SiC on cubic SiC by intentional polytype control, J. Cryst. Growth 99 (1990) 278–283.

[16] S. Lin, Z. Chen, B. Liu, L. Li, X. Feng, Identification and control of SiC polytypes in PVT method, J. Mater. Sci.: Mater. Electron. 21 (2010) 326–330.

[17] W.F. Knippenberg, Growth phenomena in silicon carbide, Philips Res. Rep. 18 (1963) 161–274.

[18] Y. Inomata, A. Inoue, M. Mitomo, H. Suzuki, Relation between growth temperature and the structure of SiC crystals grown by the sublimation method, Yogyo-Kyokai-Shi 76 (1968) 313–319.

[19] P. Krishna, R.C. Marshall, The structure, perfection and annealing behaviour of SiC needles grown by a VLS mechanism, J. Cryst. Growth 9 (1971) 319–325.

[20] T. Muranaka, Y. Kikuchi, T. Yoshizawa, N. Shirakawa, J. Akimitsu, Superconductivity in carrier-doped silicon carbide, Sci. Technol. Adv. Mater. 9 (2008) 044204.

[21] R.A. Stein, P. Lanig, S. Leibenzeder, Control of polytype formation by surface energy effects during the growth of SiC monocrystals by the sublimation method, J. Cryst. Growth 131 (1993) 71–74.

[22] A.A. Maltsev, A.Yu. Maksimov, N.K. Yushin, 4H-SiC single crystal ingots grown on 6H-SiC and 15R-SiC seeds, Inst. Phys. Conf. Ser. 142 (1996) 41.

[23] M. Kanaya, J. Takahashi, Y. Fujiwara, A. Moritani, Controlled sublimation growth of single crystalline 4H-SiC and 6H-SiC and identification of polytypes by x-ray diffraction, Appl. Phys. Lett. 58 (1991) 56–58.

[24] K. Chourou, M. Anikin, J.M. Bluet, V. Lauer, G. Guillot, J. Camassel, S. Juillaguet, O. Chaix, M. Pons, R. Madar, Experimental Investigation of 4H-SiC bulk crystal growth, Mater. Sci. Forum 264–268 (1998) 17–20.

[25] V.D. Heydemann, N. Schultze, D.L. Barrett, G. Pensl, Growth of 6H and 4H silicon carbide single crystals by the modified Lely process utilizing a dual-seed crystal method, Appl. Phys. Lett. 69 (1996) 3728–3730.

[26] Y.M. Tairov, V.F. Tsvetkov, Progress in cotrolling the growth of polytypic crystals, in: P. Krishna (Ed.), Progress in Crystal Growth and Characterization, 7, Pergamon, Oxford, New York, 1983, pp. 111–162.

[27] O.O. Mykhaylyk, M.P. Gadzira, Arrangement of C atoms in the SiC-C solid solution, Acta Crystallogr., Sec. B 55 (1999) 297–305.

[28] M. Mitomo, Y. Inomata, M. Kumanomido, The effect of doped aluminum on thermal stability of 4H- and 6H-SiC, Yogyo-Kyokai Shi 78 (1970) 224–228.

[29] S. Honda, T. Nagano, K. Kaneko, H. Kodama, Compressive deformation behavior of Al-doped β-SiC at elevated temperature, J. Eur. Ceram. Soc. 22 (2002) 979–985.

[30] B. Song, H. Bao, M. Lei, T. Peng, J. Jian, J. Liu, W. Wang, W. Wang, X. Chen, Observation of glassy ferromagnetism in Al-doped 4H-SiC, J. Am. Chem. Soc. 131 (2009) 1376–1377.

[31] B. Song, X.L. Chen, J.C. Han, G. Wang, H.Q. Bao, L.B. Duan, K.X. Zhu, H. Li, Z.H. Zhang, W.Y. Wang, W.J. Wang, X.H. Zhang, S.H. Meng, Raman scattering and magnetizations studies of (Al,Cr)-codoped 4H-SiC, J. Magn. Magn. Mater. 323 (2011) 2876–2882.

[32] K. Fekade, M.G. Spencer, K. Irvine, A.K. Ballal, D.P. Besabathina, L.G. Salamanca-Riba, TEM study of low-temperature CVD silicon carbide films grown on on-axis 6H-SiC substrates, Inst. Phys. Conf. Ser. 137 (1994) 287–295.

[33] J. Chen, S.C. Lien, Y.C. Shin, Z.C. Feng, C.H. Kuan, J.H. Zhao, W.J. Lu, Occurrence of polytype transformation during nitrogen doping of SiC bulk wafer, Mater. Sci. Forum 600-603 (2009) 39–42.

[34] N. Ohtani, M. Katsuno, M. Nakabayashi, T. Fujimoto, H. Tsuge, H. Yashiro, T. Aigo, H. Hirano, T. Hoshino, K. Tatsumi, Investigation of heavily nitrogen-doped n^+ 4H-SiC crystals grown by physical vapor transport, J. Cryst. Growth 311 (2009) 1475–1481.

[35] M. Katsuno, N. Ohtani, J. Takahashi, H. Yashiro, M. Kanaya, S. Shinoyama, Abstracts of the international workshop on hard electronics, Tsukuba (1997) 5.

[36] S. Lin, Z. Chen, X. Feng, Y. Yang, L. Li, Z. Wang, P. Pan, J. Wan, H. Wang, Y. Ba, Y. Ma, Q. Li, Observation of polytype stability in different-impurities-doped 6H-SiC crystals, Diamond Relat. Mater. 20 (2011) 516–519.

[37] S.K. Lilov, Yu.M. Tairov, V.F. Tsevtkov, M.A. Chenov, Structural and morphological peculiarities of the epitaxial layers and monocrystals of silicon carbide highly doped by nitrogen, Phys. Status Solidi A 37 (1976) 143–150.

[38] A.A. Lebedev, Influence of native defects on polytypism in SiC, Semiconductors 33 (1999) 707–709.

[39] T. Ito, T. Kondo, T. Akiyama, K. Nakamura, Theoretical investigations of the polytypism in silicon carbide: contribution of the vacancy formation, Phys. Status Solidi C 8 (2011) 583–585.

[40] L.J. Brillson, S. Tumakha, G.H. Jessen, R.S. Okojie, M. Zhang, P. Pirouz, Thermal and doping dependence of 4H-SiC polytype transformation, Appl. Phys. Lett. 81 (2002) 2785–2787.

[41] E. Pearson, T. Takai, T. Halicioglu, W.A. Tiller, Computer modeling of Si and SiC surfaces and surface processes relevant to crystal growth from the vapor, J. Cryst. Growth 70 (1984) 33–40.

[42] J. Tersoff, Modeling solid-state chemistry: interatomic potentials for multicomponent systems, Phys. Rev. B 39 (1989) 5566–5568.

[43] R. Devanathan, T. Diaz de la Rubia, W.J. Weber, Displacement threshold energies in b-SiC, J. Nucl. Mater. 253 (1998) 47–52.

[44] J. Tersoff, Carbon defects and defect reactions in silicon, Phys. Rev. Lett. 64 (1990) 1757–1760.

[45] J. Tersoff, Chemical order in amorphous silicon carbide, Phys. Rev. B 49 (1994) 16349–16352.

[46] A.J. Dyson, P.V. Smith, Extension of the Brenner empirical interatomic potential to C–Si–H systems, Surf. Sci. 355 (1996) 140–150.

[47] F. Gao, W.J. Weber, Empirical potential approach for defect properties in 3C–SiC, Nucl. Instrum. Methods Phys. Res. B 191 (2002) 504–508.

[48] R. Devanathan, F. Gao, W.J. Weber, Atomistic modeling of amorphous silicon carbide using a bond-order potential, Nucl. Instrum. Methods Phys. Res. B 255 (2007) 130–135.

[49] F. Gao, Y. Zhang, M. Posselt, W.J. Weber, Atomic-level simulations of epitaxial recrystallization and amorphous-to-crystalline transition in 4H-SiC, Phys. Rev. B 74 (2006) 104108.

[50] H. Huang, N.M. Ghoniem, J.K. Wong, M.I. Baskes, Molecular dynamics determination of defect energetics in β-SiC using three representative empirical potentials, Modell. Simul. Mater. Sci. Eng. 3 (1995) 615–627.

[51] P. Erhart, K. Albe, Analytical potential for atomistic simulations of silicon, carbon, and silicon carbide, Phys. Rev. B 71 (2005) 035211.

[52] B.J. Lee, M.I. Baskes, Second nearest-neighbor modified embedded-atom-method potential, Phys. Rev. B 62 (2000) 8564–8567.

[53] B.J. Lee, W.S. Ko, H.K. Kim, E.H. Kim, The modified embedded-atom method interatomic potentials and recent progress in atomistic simulations, CALPHAD 34 (2010) 510–522.

[54] B.J. Lee, A modified embedded atom method interatomic potential for silicon, CALPHAD 31 (2007) 95–104.

[55] B.J. Lee, J.W. Lee, A modified embedded atom method interatomic potential for carbon, CALPHAD 29 (2005) 7–16.

[56] A.R. Verma, R. Krishna, Polymorphism and Polytypism in Crystals, Wiley, New York (1966) 103.

[57] J. Gröbner, H.L. Lukas, F. Aldinger, Thermodynamic calculation of the ternary system Al–Si–C, CALPHAD 20 (1996) 247–254.

[58] W.R.L. Lambrecht, B. Segall, M. Methfessel, M. van Schilfgaarde, Calculated elastic constants and deformation potentials of cubic SiC, Phys. Rev. B 44 (1991) 3685–3694.

[59] R.E. Taylor, H. Groot, J. Ferrier, Purdue University Thermophysical Properties Research Laboratory Report no. TPRL 1336, 1993 (unpublished).

[60] Z. Li, C. Bradt, Thermal expansion of the cubic (3C) polytype of SiC, J. Mater. Sci. 21 (1986) 4366–4368.

[61] Y. Goldberg, M.E. Levinshtein, S.L. Rumyantsev, in: E. Levinshtein, S.L. Rumyantsev, M.S. Shur (Eds.), Properties of Advanced Semiconductor Materials GaN, AlN, SiC, BN, SiC, SiGe, John Wiley & Sons, Inc., New York, 2001, p. 93.

[62] R.W. Olesinski, G.J. Abbaschian, The C–Si (carbon–silicon) system, Bull. Alloy Phase Diag. 5 (1984) 486–489.

[63] A. Taylor, R.M. Jones, in: J. Smiltens O'Connor (Ed.), Silicon Carbide—A High Temperature Semiconductor, Pergamon, Oxford, London, New York, Paris, 1960, p. 147.

[64] T.C. Chiang, J. Dumas, Y.R. Shen, Brillouin-scattering in layer compound GaSe, Solid State Commun. 28 (1978) 173–176.

[65] G. Arlt, G.R. Schodder, Some elastic constants of silicon carbide, J. Acoust. Soc. Am. 37 (1965) 384–386.

[66] K. Kamitani, M. Grimsditch, J.C. Nipko, C.K. Loong, M. Okada, I. Kimura, The elastic constants of silicon carbide: a Brillouin-scattering study of 4H and 6H SiC single crystals, J. Appl. Phys. 82 (1997) 3152–3154.

[67] S. Karmann, R. Helbig, R.A. Stein, Piezoelectric properties and elastic constants of 4H and 6H SiC at temperatures 4–320 K, J. Appl. Phys. 66 (1989) 3922–3924.

[68] R. Rouka, J. Tolle, A.V.G. Chizmeshya, P.A. Crozier, C.D. Poweleit, D.J. Smith, I.S. T. Tsong, J. Kouvetakis, Low-temperature epitaxial growth of the quaternary wide band gap semiconductor SiCAlN, Phys. Rev. Lett. 88 (2002) 206102.

[69] H. Schulz, K.H. Thiemann, Structure parameters and polarity of the wurtzite type compounds SiC-2H and ZnO, Solid State Commun. 32 (1979) 783–785.

[70] K. Karch, P. Pavone, W. Windl, O. Schütt, D. Strauch, Ab initio calculation of structural and lattice-dynamical properties of silicon carbide, Phys. Rev. B 50 (1994) 17054–17063.

[71] C.Z. Wang, R. Yu, H. Krakauer, Pressure dependence of Born effective charges, dielectric constant, and lattice dynamics in SiC, Phys. Rev. B 53 (1996) 5430–5437.

[72] M. Prikhodko, M. Miao, W.R.L. Lambrecht, Pressure dependence of sound velocities in 3C-SiC and their relation to the high-pressure phase transition, Phys. Rev. B 66 (2002) 125201.

[73] A. Isik, Ph.D. thesis, Massachusetts Institute of Technology, 1994.

[74] C.H. Park, B.H. Cheong, K.H. Lee, K.J. Chang, Structural and electronic properties of cubic, 2H, 4H, and 6H SiC, Phys. Rev. B 49 (1994) 4485–4493.

[75] E. Konstantinova, M.J.V. Bell, V. Anjos, Ab initio calculations of some electronic and elastic properties for SiC polytypes, Intermetallics 16 (2008) 1040–1042.

[76] P. Käckell, B. Wenzien, F. Bechstedt, Influence of atomic relaxations on the structural properties of SiC polytypes from ab initio calculations, Phys. Rev. B 50 (1994) 17037–17046.

[77] K. Karch, G. Wellenhofer, P. Pavone, U. Rössler, D. Strauch, in: Proceedings of the 22nd International Conference on the Physics of Semiconductors, in: D. Lockwood (Eds.), World Scientific, Singapore, 1995, pp. 401.

[78] S. Limpijumnong, W.R.L. Lambrecht, Total energy differences between SiC polytypes revisited, Phys. Rev. B 57 (1998) 12017–12022.

[79] A.P. Mirgorodsky, M.B. Smirnov, E. Abdelmounim, T. Merle, P.E. Quintard, Molecular approach to the modeling of elasticity and piezoelectricity of SiC polytypes, Phys. Rev. B 52 (1995) 3993–4000.

[80] K. Kobayash, S. Komatsu, First-principles study of BN, SiC, and AlN polytypes, J. Phys. Soc. Jpn. 77 (2008) 084703.

[81] V. Heine, C. Cheng, G.E. Engel, R.J. Needs, Wide band gap semiconductors, in: T.D. Moustakas, J.I. Pankove, and Y. Hamakawa (Eds.), MRS Symposia Proceedings No. 242, Materials Research Society, Pittsburgh, 1992, pp. 507.

[82] V. Heine, C. Cheng, R.J. Needs, A computational study into the origin of SiC polytypes, Mater. Sci. Eng. B 11 (1992) 55.

[83] K. Strössner, M. Cardona, High pressure X-ray investigations on 3C-SiC, Solid State Commun. 63 (1987) 113–114.

[84] M. Yoshida, A. Onodera, M. Ueno, K. Takemura, O. Shimomura, Pressure-induced phase transition in SiC, Phys. Rev. B 48 (1993) 10587–10590.

[85] W.A. Bassett, M.S. Weathers, T.C. Wu, Compressibility of SiC up to 66.4 GPa, J. Appl. Phys. 74 (1993) 3824–3826.

[86] R. Ramírez, C.P. Herrero, E.R. Hernández, M. Cardona, Path-integral molecular dynamics simulation of 3C-SiC, Phys. Rev. B **77** (2008) 045210.

[87] M.J. Tang, S. Yip, Atomistic simulation of thermomechanical properties of β-SiC, Phys. Rev. B 52 (1995) 15150–15159.

[88] F. Shimojo, I. Ebbsjö, R.K. Kalia, A. Nakano, J.P. Rino, P. Vashishta, Molecular dynamics simulation of structural transformation in silicon carbide under pressure, Phys. Rev. Lett. 84 (2000) 3338–3341.

[89] J. Droward, G. De Maria, M.G. Inghram, Thermodynamic study of SiC utilizing a mass spectrometer, J. Chem. Phys. 29 (1958) 1015–1021.

[90] S.A. Sakwe, M. Stockmeier, P. Hens, R. Müller, D. Queren, U. Kunecke, K. Konias, R. Hock, A. Magerl, M. Pons, A. Winnacker, P. Wellmann, Bulk growth of SiC—review on advances of SiC vapor growth for improved doping and systematic study on dislocation evolution, Phys. Status Solidi B 245 (2008) 1239–1256.

[91] L. Kaufman, H. Bernstein, Computer Calculation of Phase Diagrams with Special Reference to Refractory Metals, Academic, New York, 1970.

[92] H.L. Lukas, S.G. Fries, B. Sundman, Computational Thermodynamics, Cambridge University, New York, 2007.

[93] B. Sundman, B. Jansson, J.O. Anderson, The thermo-calc databank system, CALPHAD 9 (1985) 153–190.

[94] SUB97: SGTE substance database, ⟨http://www.sgte.org/⟩.

[95] N. Jegenyes, M. Marinova, G. Zoulis, J. Lorenzzi, A. Andreadou, A. Mantzari, V. Soulière, S. Juillaguet, J. Camassel, E.K. Polychroniadis, G. Ferro, Influence of the C/Si ratio on the dopant concentration and defects in CVD grown 3C-SiC homoepitaxial layers, AIP Conf. Proc. 1292 (2010) 31–34.

[96] T. Ohno, H. Yamaguchi, S. Kuroda, K. Kojima, T. Suzuki, K. Arai, Influence of growth conditions on basal plane dislocation in 4H-SiC epitaxial layer, J. Cryst. Growth 271 (2004) 1–7.

[97] G. Kresse, D. Joubert, From ultrasoft pseudopotentials to the projector augmented-wave method, Phys. Rev. B 59 (1999) 1758–1775.

[98] P. Hohenberg, W. Kohn, Inhomogeneous electron gas, Phys. Rev. 136 (1964) B864–B871.

[99] J.P. Perdew, K. Burke, M. Ernzerhof, Generalized gradient approximation made simple, Phys. Rev. Lett. **77** (1996) 3865–3868.

[100] F. Gao, E.J. Bylaska, W.J. Weber, R. Corrales, Ab initio and empirical-potential studies of defect properties in 3C-SiC, Phys. Rev. B 64 (2001) 245208.

[101] C. Wang, J. Bernholc, R.F. Davis, Formation energies, abundances, and the electronic structure of native defects in cubic SiC, Phys. Rev. B 38 (1988) 12752–12755.

[102] A. Gali, P. Deák, P. Ordejón, N.T. Son, E. Janzén, W.J. Choyke, Aggregation of carbon interstitials in silicon carbide: a theoretical study, Phys. Rev. B 68 (2003) 125201.

[103] V.A. Gubanov, C.Y. Fong, Doping in cubic silicon-carbide, Appl. Phys. Lett. 75 (1999) 88–90.

[104] L. Wang, S. Dimitrijev, J. Han, P. Tanner, A. Lacopi, L. Hold, Demonstration of p-type 3C–SiC grown on 150 mm Si(100) substrates by atomic-layer epitaxy at 1000 °C, J. Cryst. Growth 329 (2001) 67–70.